J|A|C|S
ARTICLES
Published on Web 04/05/2003

Resonance Raman Investigation of Equatorial Ligand Donor Effects on the $Cu_2O_2^{2+}$ Core in End-On and Side-On μ-Peroxo-Dicopper(II) and Bis-μ-oxo-Dicopper(III) Complexes

Mark J. Henson,[†,§] Michael A. Vance,[†,§] Christiana Xin Zhang,[‡] Hong-Chang Liang,[‡] Kenneth D. Karlin,*[,‡] and Edward I. Solomon*[,†]

Contribution from the Department of Chemistry, Stanford University, Stanford, California 94305-5080 and Department of Chemistry, The Johns Hopkins University, 3400 North Charles Street, Baltimore, Maryland 21218

Received July 10, 2002; E-mail: Edward.Solomon@stanford.edu; karlin@jhu.edu

Abstract: The effect of endogenous donor strength on Cu_2O_2 bonds was studied by electronically perturbing $[\{(R-TMPA)Cu^{II}\}_2(O_2)]^{2+}$ and $[\{(R-MePY2)Cu\}_2(O_2)]^{2+}$ (R = H, MeO, Me_2N), which form the end-on μ-1,2 bound peroxide and an equilibrium mixture of side-on peroxo-dicopper(II) and bis-μ-oxo-dicopper(III) isomers, respectively. For $[\{(R\text{-}TMPA)Cu^{II}\}_2(O_2)]^{2+}$, ν_{O-O} shifts from 827 to 822 to 812 cm^{-1} and $\nu_{Cu-O(sym)}$ shifts from 561 to 557 to 551 cm^{-1}, respectively, as R− varies from H to MeO to Me_2N. Thus, increasing the N-donor strength to the copper decreases peroxide π^*_σ donation to the copper, weakening the Cu−O and O−O bonds. A decrease in ν_{Cu-O} of the bis-μ-oxo-dicopper(III) complex was also observed with increasing N-donor strength for the R−MePY2 ligand system. However, no change was observed for ν_{O-O} of the side-on peroxo. This is attributed to a reduced charge donation from the peroxide π^*_σ orbital with increased N-donor strength, which increases the negative charge on the peroxide and adversely affects the back-bonding from the Cu to the peroxide σ^* orbital. However, an increase in the bis-μ-oxo-dicopper(III) isomer relative to side-on peroxo-dicopper(II) species is observed for R−MePY2 with R = H < MeO < Me_2N. This effect is attributed to the thermodynamic stabilization of the bis-μ-oxo-dicopper(III) isomer relative to the side-on peroxo-dicopper(II) isomer by strong donor ligands. Thus, the side-on peroxo-dicopper(II)/bis-μ-oxo-dicopper(III) equilibrium can be controlled by *electronic as well as steric effects*.

Introduction

Binuclear copper centers play important roles in the bioinorganic chemistry of dioxygen.[1,2] Hemocyanin is a coupled binuclear copper protein in the hemolymph of arthropods and mollusks which reversibly binds and transports dioxygen. Catechol oxidase catalyzes the oxidation of catechols to *o*-quinones (cresolase reaction).[3] Tyrosinase catalyzes catechol oxidation but additionally hydroxylates phenols to catechols.[1,4] The *o*-quinones produced by both enzymes rapidly polymerize to form the skin pigment melanin. This process is also involved in wound protection via the browning reaction of fruits and vegetables as well as in insect sclerotization.

Despite the disparate reactivity found in these systems, the coupled binuclear copper(II) active sites are remarkably similar in both geometric structure[1,3,5−7] and spectroscopic features.[8−10] Each copper is coordinated by three histidines, one of which is an axial ligand with an elongated Cu(II)−N bond (∼2.3 Å). Dioxygen binds between the two copper(II) centers as peroxide (r_{O-O} = 1.4 Å) in a side-on, μ-η^2:η^2 configuration with a Cu−Cu distance of 3.6−3.8 Å for oxyhemocyanin.[5−7]

A large number of systems have been synthesized that model the binuclear copper active site.[1,8,11−21] Spectroscopic investiga-

[†] Stanford University.
[‡] The Johns Hopkins University.
[§] These authors contributed equally to this work.

(1) Solomon, E. I.; Sundaram, U. M.; Machonkin, T. E. *Chem. Rev.* **1996**, *96*, 2563.
(2) Solomon, E. I.; Chen, P.; Metz, M.; Lee, S.-K.; Palmer, A. E. *Ang. Chem., Int. Ed.* **2001**, *40*, 4570.
(3) Tremolieres, M.; Bieth, J. G. *Phytochemistry* **1984**, 501.
(4) Gerdemann, C.; Eicken, C.; Krebs, B. *Acc. Chem. Res.* **2002**, *35*, 183.
(5) Magnus, K. A.; Tonthat, H.; Carpenter, J. E. *Chem. Rev.* **1994**, *94*, 727.
(6) Magnus, K. A.; Hazes, B.; Tonthat, H.; Bonaventura, C.; Bonaventura, J.; Hol, W. G. J.; Dauter, Z.; Kalk, K. H. *Proteins: Struct., Funct., Genet.* **1994**, 302.
(7) Klabunde, T.; Eicken, C.; Sacchettini, J. C.; Krebs, B. *Nat. Struct. Biol.* **1998**, *5*, 1084.
(8) Solomon, E. I.; Tuczek, F.; Root, D. E.; Brown, C. A. *Chem. Rev.* **1994**, *94*, 827.
(9) Rompel, A.; Fischer, H.; Meiwes, D.; Buldtkarentzopoulos, K.; Dillinger, R.; Tuczek, F.; Witzel, H.; Krebs, B. *J. Biol. Inorg. Chem.* **1999**, *4*, 56.
(10) Jolley, R. L.; Evans, L. H.; Mason, H. S. *Biochem. Biophys. Res. Commun.* **1972**, *46*, 878.
(11) Que, L., Jr.; Tolman, W. B. *Ang. Chem., Int. Ed.* **2002**, *41*, 1114.
(12) Blackman, A. G.; Tolman, W. B. *Struct. Bonding* **2000**, *97*, 179.
(13) Schindler, S. *Eur. J. Inorg. Chem.* **2000**, 2311.
(14) Suzuki, M.; Furutachi, H.; Okawa, H. *Coord. Chem. Rev.* **2000**, *200*, 105.
(15) Zhang, C. X.; Liang, H.-C.; Humphreys, K. J.; Karlin, K. D. In *Advances in Catalytic Activation of Dioxygen by Metal Complexes*; Simandi, L., Ed.; Kluwer Academic Publishers: Dordrecht, The Netherlands, 2003; Vol. 26, p 79.
(16) Liang, H.-C.; Zhang, C. X.; Henson, M. J.; Sommer, R. D.; Hatwell, K. R.; Kaderli, S.; Zuberbuehler, A. D.; Rheingold, A. L.; Solomon, E. I.; Karlin, K. D. *J. Am. Chem. Soc.* **2002**, *124*, 4170.
(17) Karlin, K. D.; Zuberbühler, A. D. In *Bioinorganic Catalysis: Second Edition, Revised and Expanded*; Reedijk, J., Bouwman, E., Eds.; Marcel Dekker: New York, 1999; p 469.
(18) Spencer, D. J. E.; Aboelella, N. W.; Reynolds, A. M.; Holland, P. L.; Tolman, W. B. *J. Am. Chem. Soc.* **2002**, *124*, 2108.
(19) Taki, M.; Teramae, S.; Nagatomo, S.; Tachi, Y.; Kitagawa, T.; Itoh, S.; Fukuzumi, S. *J. Am. Chem. Soc.* **2002**, *124*, 6367.

 10.1021/ja0276366 CCC: $25.00

Chart 1

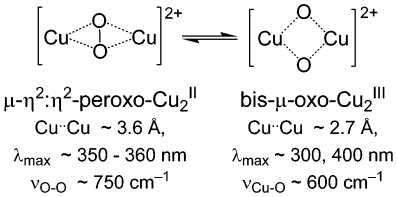

Scheme 1

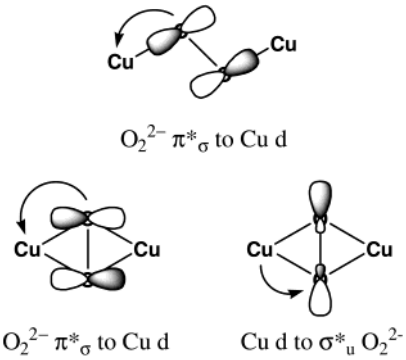

tions have shown that the side-on peroxo-dicopper(II) complex can exist in rapid equilibrium with an isomeric form of the Cu_2O_2 core, a bis-μ-oxo-dicopper(III) complex (Chart 1).[11] The equilibrium constant for interconversion of the side-on peroxo and bis-μ-oxo isomers has been shown to be dependent upon concentration, temperature, ligand steric bulk, and the coordinating ability of the solvent and/or the counterion.[11−16,22−24] While several studies have explored the influence of amine ligand sterics upon the equilibrium constant, little research has been directed toward determining the influence of electronic effects, which are also directly responsible for the unique spectroscopic features and reactivity of the side-on peroxo-dicopper(II) isomeric species. Back-donation from the Cu(II) ions into the O_2^{2-} σ^*_u orbital (Scheme 1, bottom right) weakens the O−O bond (reflected in the low $\nu_{O-O} = \sim 750$ cm^{-1} in the resonance Raman spectrum), activating it for cleavage.[25,26] With sufficient donation into the σ^*_u orbital, the O−O bond is reductively cleaved to form the bis-μ-oxo-dicopper(III) isomer.[27]

Model studies have also produced a Cu_2O_2 complex where dioxygen is bridged end-on (μ-1:2).[28] In the TMPA (TMPA = tris(2-methylpyridyl)amine)) coupled binuclear Cu(II) system, which binds O_2 as an end-on μ-1,2 peroxide (Scheme 2, top), back-donation from Cu(II) to the O_2^{2-} σ^*_u orbital does not occur and peroxide acts only as a σ donor using the π^*_σ orbitals (Scheme 1, top).[29] This σ donation is also present and much stronger in the side-on bridged structure as peroxide makes two σ bonds to each of the two coppers (Scheme 1, bottom left).[30]

Scheme 2

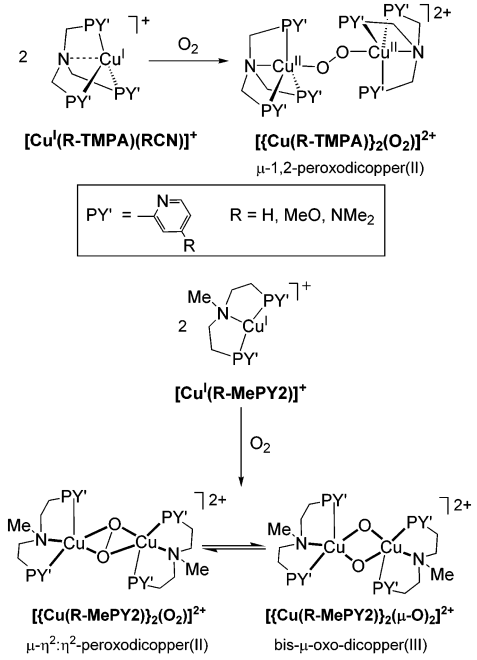

In this study, we present resonance Raman results for Cu_2O_2 systems in which the spectroscopic features of the side-on peroxo-dicopper(II)/bis-μ-oxo-dicopper(III) equilibrium are electronically, rather than sterically, controlled. The electronic donor strength of the ligand R−MePY2 is systematically increased by varying the R-substituent (R = H, MeO, Me_2N), which controls the side-on peroxo-dicopper(II)/bis-μ-oxo-dicopper(III) equilibrium (Scheme 2, bottom). These results are compared and contrasted to those of the end-on bridged R−TMPA complexes (R = H, MeO, Me_2N). These studies define the effects of endogenous donor strength on Cu−O and O−O bonds.

Experimental Section

Sample Preparation. Full synthetic details for the TMPA and MePY2 series of ligands and copper (I) complexes have been described elsewhere.[31,32] An abbreviated description appears in the Supporting Information. Compounds are referred to in the text just in terms of their cationic portions; complexes were prepared as tetraarylborate salts, either with a tetrakis[3,5-bis(trifluoromethyl)phenyl]borate counterion (=BArF) or with a $B(C_6F_5)^{4-}$ counterion (=BArF′). The following complexes were utilized in the present study: from the R−TMPA series, [(TMPA)Cu(I)(MeCN)]BArF, [(MeO−TMPA)Cu(I)(MeCN)]BArF, [(Me_2N−TMPA)Cu(I)]BArF; from the R−MePY2 series, [(MePY2)Cu(I)(MeCN)]BArF′, [(MeO−MePY2)Cu(I)(MeCN)]BArF′, [(Me_2N−MePY2)Cu(I)(MeCN)]BArF′.

Resonance Raman. Resonance Raman (rR) spectra were obtained using a Princeton Instruments ST-135 back-illuminated CCD detector on a Spex 1877 CP triple monochromator with 1200, 1800, and 2400 grooves/mm holographic spectrograph gratings. Excitation was provided by Coherent I90C-K Kr^+ and Innova Sabre 25/7 Ar^+ CW ion lasers. Laser lines were chosen to coincide with the intense absorption transitions of the different Cu_2O_2 species listed in Table 1. Spectral resolution was < 2 cm^{-1}.

(20) Mirica, L. M.; Vance, M.; Rudd, D. J.; Hedman, B.; Hodgson, K. O.; Solomon, E. I.; Stack, T. D. P. *J. Am. Chem. Soc.* **2002**, *124*, 9332.
(21) Holland, P. L.; Cramer, C. J.; Wilkinson, E. C.; Mahapatra, S.; Rodgers, K. R.; Itoh, S.; Taki, M.; Fukuzumi, S.; Que, L.; Tolman, W. B. *J. Am. Chem. Soc.* **2000**, *122*, 792.
(22) Halfen, J. A.; Mahapatra, S.; Wilkinson, E. C.; Kaderli, S.; Young, V. G.; Que, L.; Zuberbuhler, A. D.; Tolman, W. B. *Science* **1996**, *271*, 1397.
(23) Mahadevan, V.; Henson, M. J.; Solomon, E. I.; Stack, T. D. P. *J. Am. Chem. Soc.* **2000**, *122*, 10249.
(24) Cahoy, J.; Holland, P. L.; Tolman, W. B. *Inorg. Chem.* **1999**, *38*, 2161.
(25) Ross, P. K.; Solomon, E. I. *J. Am. Chem. Soc.* **1990**, *112*, 5871.
(26) Ross, P. K.; Solomon, E. I. *J. Am. Chem. Soc.* **1991**, *113*, 3246.
(27) Henson, M. J.; Mukherjee, P.; Root, D. E.; Stack, T. D. P.; Solomon, E. I. *J. Am. Chem. Soc.* **1999**, *121*, 10332.
(28) Jacobson, R. R.; Tyeklar, Z.; Farooq, A.; Karlin, K. D.; Liu, S. C.; Zubieta, J. *J. Am. Chem. Soc.* **1988**, *111*, 3690.
(29) Baldwin, M. J.; Ross, P. K.; Pate, J. E.; Tyeklar, Z.; Karlin, K. D.; Solomon, E. I. *J. Am. Chem. Soc.* **1991**, *113*, 8671.
(30) Baldwin, M. J.; Root, D. E.; Pate, J. E.; Fujisawa, K.; Kitajima, N.; Solomon, E. I. *J. Am. Chem. Soc.* **1992**, *114*, 10421.
(31) Zhang, C. X.; Liang, H. C.; Kim, E.-I.; Shearer, J.; Helton, M. E.; Kim, E.; Kaderli, S.; Incarvito, C. D.; Rheingold, A. L.; Zuberbuehler, A. D.; Karlin, K. D. *J. Am. Chem. Soc.* **2003**, *125*, 634.
(32) Zhang, C. X.; Kaderli, S.; Costas, M.; Kim, E.-I.; Neuhold, Y.-M.; Karlin, K. D.; Zuberbuehler, A. D. *Inorg. Chem.* **2003**, *42*, 1807−1824. Web release February 12 2003.

Table 1. Absorption Maxima for the Dioxygen Bound R−MePY$_2$ (in CH_2Cl_2) and R−TMPA Series (Et_2O)

	H			MeO			Me_2N		
R =	λ (nm)	energy (cm^{-1})	ϵ ($cm^{-1}\,M^{-1}$)	λ (nm)	energy (cm^{-1})	ϵ ($cm^{-1}\,M^{-1}$)	λ (nm)	energy (cm^{-1})	ϵ ($cm^{-1}\,M^{-1}$)
MePY2	356	28 100	14 800	356	28 100	20 000	360	27 800	21 000
	410	24 400	2900	410	24 400	3500	~410[a]	~24 400	
	530	18 900	570	535	18 700	1000	515	19 400	1400
	654	15 300	460	650	15 400	750	650	15 400	730
TMPA	520	19 200	~14 000	520	19 200	~15 000	523	19 100	~11 000

[a] This peak exists as a shoulder on the 360 nm absorption peak.

The samples were prepared by dissolving the Cu(I) amine precursor in solvent in 5 mm NMR tubes and oxygenating at −80 °C. Typical rR solution sample concentrations were in the range of 2−5 mM of Cu (1−2.5 mM of dimer) to minimize self-absorption. The samples were cooled to 77 K in a quartz liquid N_2 EPR finger dewar (Wilmad) and hand spun during scan collection to minimize sample decomposition. Isotopic substitution was achieved by oxygenation with $^{18}O_2$ (ICON, 99% labeled).

Computational Details. Normal coordinate analysis (NCA) was performed on a simplified $[(N_2Cu)_2O_2]$ complex by using QCPE program 576 by M. R. Peterson and D. F. McIntosh, which involves solution of the secular equation $|\mathbf{FG} - \lambda\mathbf{E}| = 0$[33,34] by the diagonalization procedure of Miyazawa.[35] The calculations were based on a general valence force field. Force constants were refined with the nonlinear optimization routine of the simplex algorithm according to Nelder and Mead.[36] Input data sets can be found and additional NCA details can be found in the Supporting Information.

DFT calculations were performed with the program package Gaussian 98[37] using the BP86 functional[38] (modified to include 38% Hartree−Fock exchange) and the LANL2DZ basis set.[39−42] A geometry optimized $[\{(NH_3)_3Cu^{II}\}_2(O_2)]^{2+}$ structure in the broken symmetry and delocalized singlet spin states (the delocalized singlet was calculated to directly evaluate the effect of N-donor strength on the peroxide σ^*_u orbital; this mixed orbital is dominated by π^*_σ interaction in the broken symmetry calculation) was used as a control. Replacement of the histidine ligands by ammonia ligands is supported by previous studies.[25,26] Increased N-donor strength was modeled by shortening the equatorial Cu−N bonds by 0.05 Å and performing a single-point calculation. Input data sets are given in the Supporting Information.

Results and Analysis

R−TMPA. The resonance Raman (rR) spectrum of $^{16}O_2$ bound $[\{(MeO-TMPA)Cu^{II}\}_2(O_2)]^{2+}$ in diethyl ether (Et_2O) for $\lambda_{ex} = 514.5$ nm shows two main peaks which display isotope shifts upon $^{18}O_2$ substitution (Figure 1, inset). The intense peak

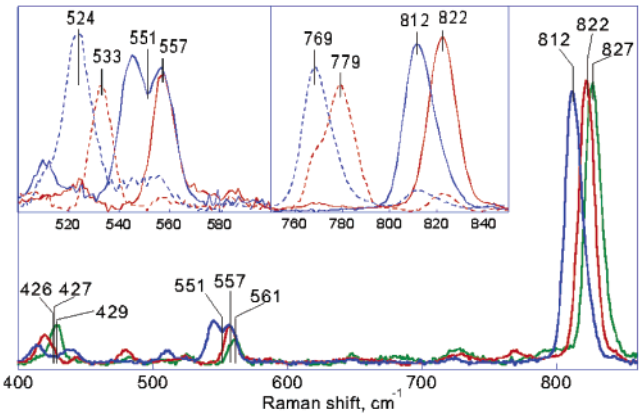

Figure 1. Resonance Raman spectra (77 K) of the $[\{(R-TMPA)Cu^{II}\}_2(O_2)]^{2+}$ series in Et_2O for a 514 nm excitation. R = H is the green spectrum, R = MeO is the red spectrum, and R = Me_2N is the blue spectrum. See Figure S2 for an expanded view of the Cu−N_{ax} region. Inset: Resonance Raman (77 K) $^{16}O_2$ (solid line)/$^{18}O_2$(dashed line) isotopic comparison of $[\{(R-TMPA)Cu^{II}\}_2(O_2)]^{2+}$ (R = MeO, Me_2N). The solvent was Et_2O, and $\lambda_{ex} = 514$ nm. R = MeO is the red spectrum, and R = Me_2N is the blue spectrum. Note: $^{18}O_2$ spectra contain a small amount of isotopic $^{16}O_2$.

at $\nu = 822$ cm^{-1} shifts to 779 cm^{-1} ($^{16,18}\Delta = -43$ cm^{-1}), while the peak at $\nu = 557$ cm^{-1} shifts to 533 cm^{-1} ($^{16,18}\Delta = -24$ cm^{-1}). Similarly, a shift is observed in the more intense peak in the trans μ-1,2 end-on dimer $[\{(Me_2N-TMPA)Cu^{II}\}_2(O_2)]^{2+}$ spectrum (Figure 1, inset): $\nu = 812$ cm^{-1} ($^{16,18}\Delta = -43$ cm^{-1}). However, the $^{16}O_2$ $[\{(Me_2N-TMPA)Cu^{II}\}_2(O_2)]^{2+}$ spectrum shows a doublet of peaks at 545 and 557 cm^{-1} arising from a Fermi resonance (Figure 1), as this splitting is not present in the $^{18}O_2$ spectrum at 524 cm^{-1}. Averaging of the two peaks in the $^{16}O_2$ spectrum (av = 551 cm^{-1}) gives an isotope shift of −27 cm^{-1} for this feature (Figure 1, inset). These data are consistent with results on the end-on peroxo-dicopper(II) complex using the unsubstituted TMPA ligand: $\nu_{O-O} = 827$ cm^{-1} ($^{16,18}\Delta = -44$ cm^{-1}); $\nu_{Cu-O} = 561$ cm^{-1} ($^{16,18}\Delta = -26$ cm^{-1}).[29] Thus, the intense peaks at 827−812 cm^{-1} are assigned as the ν_{O-O} stretches, while the 551−561 cm^{-1} bands correspond to the symmetric combination of the Cu−O stretches. [Note that the asymmetric combination of the Cu−O stretches is also observed in the H−TMPA rR spectrum: $\nu = 525$ cm^{-1} ($^{16,18}\Delta = -19$ cm^{-1}) and $\nu = 511$ cm^{-1} ($^{16,18}\Delta = -20$ cm^{-1}), consistent with previous normal coordinate predictions for TMPA (see Supporting Information Figure S1).][29]

The Cu−N_{ax} stretch (nitrogen trans to the axial peroxo O-ligand in the trigonal bipyramidal coordination geometry) was seen at 429 cm^{-1} for $[\{(H-TMPA)Cu^{II}\}_2(O_2)]^{2+}$ (Table 2).[29] Similar stretches are observed for the $[\{(MeO-TMPA)Cu^{II}\}_2(O_2)]^{2+}$ and $[\{(Me_2N-TMPA)Cu^{II}\}_2(O_2)]^{2+}$ complexes (Figure 1). After the deconvolution of the Fermi resonance,[33] the pure Cu−N_{ax} modes are estimated to be at 427 and 426 cm^{-1},

(33) Wilson, E. B., Jr.; Decius, J. C.; Cross, P. C. *Molecular Vibrations*; Dover Publications: New York, 1980.
(34) Woodward, L. A. *Introduction to the Theory of Molecular Vibrations and Vibrational Spectroscopy*; Clarendon Press: Oxford, 1972.
(35) Miyasawa, T. *J. Chem. Phys.* **1958**, *29*, 246.
(36) Nelder, J. A.; Mead, R. *Comput. J.* **1965**, *7*, 308.
(37) Frisch, M. J.; Trucks, G. W.; Schlegel, H. B.; Scuseria, G. E.; Robb, M. A.; Cheeseman, J. R.; Zakrzewski, V. G.; Montgomery, J. A.; Strattmann, R. E.; Burant, J. C.; Dapprich, S.; Millam, J. M.; Daniels, A. D.; Kudin, K. N.; Strain, M. C.; Farkas, O.; Tomasi, J.; Barone, V.; Cossi, M.; Cammi, R.; Mennucci, B.; Pomelli, C.; Adamo, C.; Clifford, S.; Ochterski, J.; Petersson, G. A.; Ayala, P. Y.; Cui, Q.; Morokuma, K.; Malick, D. K.; Rabuck, A. D.; Raghavachari, K.; Foresman, J. B.; Cioslowski, J.; Oritz, J. V.; Stefanov, B. B.; Liu, G.; Liashenko, A.; Piskorz, P.; Komaromi, I.; Gomperts, R.; Martin, R. L.; Fox, D. J.; Keith, T.; Al-Laham, M. A.; Peng, C. Y.; Nanayakkara, A.; Gonzalez, C.; Challacombe, M.; Gill, P. M. W.; Johnson, B. G.; Chen, W.; Wong, W. M.; Andres, J. L.; Head-Gordon, M.; Replogle, E. S.; Pople, J. A. *Gaussian 98*, revision A.7; Gaussian, Inc.: Pittsburgh, PA, 1998.
(38) Perdew, J. P. *Phys. Rev. B: Condens. Matter* **1986**, *33*, 8822.
(39) Dunning, T. H. J.; Hay, P. J. In *Modern Theoretical Chemistry*; Schaefer, H. F., III, Ed.; Plenum: New York, 1976; Vol. 3, p 1.
(40) Hay, P. J.; Wadt, W. R. J. *J. Chem. Phys.* **1985**, *82*, 270.
(41) Hay, P. J.; Wadt, W. R. J. *J. Chem. Phys.* **1985**, *82*, 299.
(42) Wadt, W. R. J.; Hay, P. J. *J. Chem. Phys.* **1985**, *82*, 284.

Table 2. Resonance Raman Stretching Frequencies for the R−TMPA Ligand Series

	ν_{O-O}			ν_{Cu-O}			
	$^{16}O_2$	$^{18}O_2$	$\Delta\nu$	$^{16}O_2$	$^{18}O_2$	$\Delta\nu$	$\nu_{Cu-N_{ax}}$
R = H	827	783	44	561	535	26	429
R = MeO	822	779	43	557 (sym)	533	24	427
				525 (asym)	506	19	
R = Me_2N	812	769	43	557, 545	524	27	426
				av = 551	491	20	
				511 (asym)			

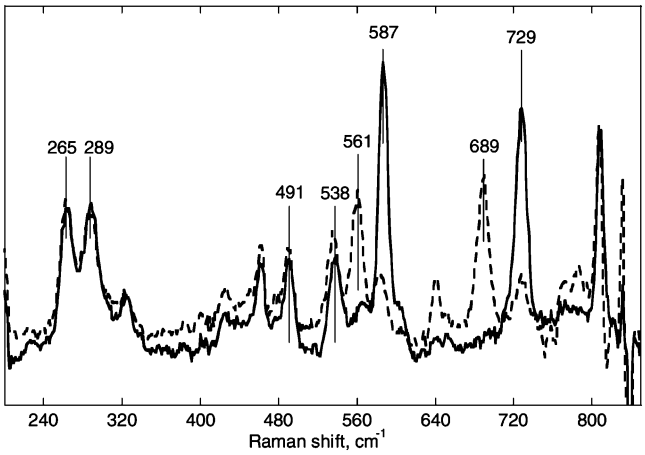

Figure 2. $^{16}O_2$ and $^{18}O_2$ isotope comparison of resonance Raman spectra of $[\{(H-MePY2)Cu\}_2(O_2)]^{2+}$ in THF-d_8 (solvent subtracted) at 77 K. Excitation at 407 nm. (——) denotes $^{16}O_2$, and (- - - - -) denotes $^{18}O_2$. Note: $^{18}O_2$ spectrum contains a small amount of isotopic $^{16}O_2$.

respectively (Table 2; see Supporting Information Figure S2 for a more detailed Cu−N_{ax} region).

Thus, the frequencies of the ν_{O-O}, ν_{Cu-O}, and $\nu_{Cu-N_{ax}}$ vibrations in the rR spectrum of R−TMPA are dependent upon the nature of the R− substituent. As the substituent is varied from H to MeO to Me_2N, the ν_{O-O} band shifts downward in frequency from 827 to 822 to 812 cm^{-1} (Figure 1, bottom). Similarly, a shift of the Cu−O and Cu−Nax vibrations to lower energy occurs over this series from 561 to 557 to 551 cm^{-1} and from 429 to 427 to 426 cm^{-1}, respectively (Figure 1; Table 2).

MePY2. The resonance Raman spectrum of $[\{(H-MePY2)Cu\}_2(O_2)]^{2+}$ in THF-d_8 (for λ_{ex} = 406.7 nm) is shown in Figure 2. The spectrum is characterized by vibrational features corresponding to both the side-on peroxo-dicopper(II) [ν_{O-O} = 729 cm^{-1} ($^{16,18}\Delta = -40$ cm^{-1}; Figure 2); ν_{Cu-Cu} = 265, 289 cm^{-1} (Figure 2; $^{16,18}\Delta = 0$ cm^{-1} for both; the observation of two ν_{Cu-Cu} peaks is discussed in the following)] and bis-μ-oxo-dicopper(III) [ν_{Cu-O} = 587 cm^{-1} ($^{16,18}\Delta = -26$ cm^{-1})] isomers. The peaks at 491 and 538 cm^{-1} are isotope independent and are in the range expected for equatorial Cu−N vibrations of a bis-μ-oxo-dicopper(III) complex.[27] The Cu−N_{PY} (equatorial pyridine nitrogen) vibration is assigned as the lower of the two vibrations given the larger mass of the pyridine ring. Thus, the 491 cm^{-1} vibration is assigned as the Cu−N_{PY} stretch, and 538 cm^{-1} is assigned as a Cu−N (equatorial tertiary nitrogen) vibration (see Figure 2). The corresponding Raman spectra of $[\{(R-MePY2)Cu\}_2(O_2)]^{2+}$ for R = MeO (Figure 3) and Me_2N (Figure 4) also contain features indicating the presence of both isomers (Table 3). For R = MeO, the side-on peroxo-dicopper-(II) species has ν_{O-O} = 728 cm^{-1} ($^{16,18}\Delta = -39$ cm^{-1}) and

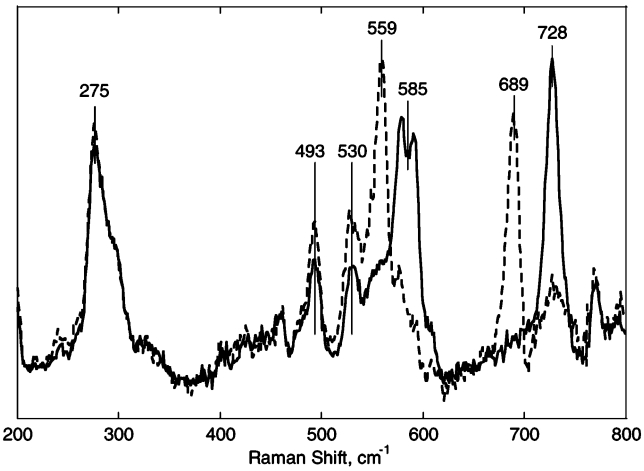

Figure 3. $^{16}O_2$ and $^{18}O_2$ isotope comparison of resonance Raman spectra of $[\{(MeO-MePY2)Cu\}_2(O_2)]^{2+}$ in THF-d_8 (solvent subtracted) at 77 K. Excitation at 407 nm. (——) denotes $^{16}O_2$, and (- - - - -) denotes $^{18}O_2$. Note: $^{18}O_2$ spectrum contains a small amount of isotopic $^{16}O_2$.

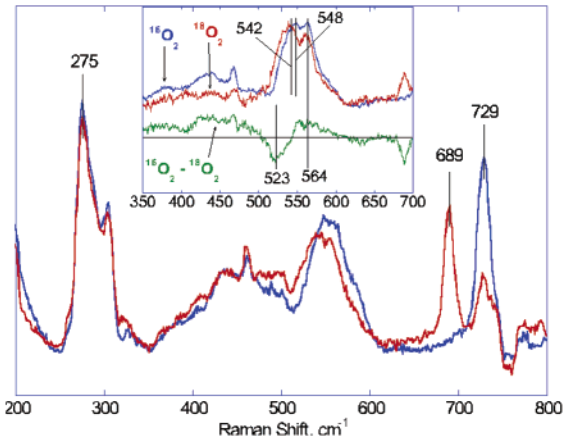

Figure 4. $^{16}O_2$ and $^{18}O_2$ isotope comparison of resonance Raman spectra of $[\{(Me_2N-MePY2)Cu\}_2(O_2)]^{2+}$ in THF-d_8 (solvent subtracted) at 77 K. Excitation at 407 nm. The red spectrum denotes $^{16}O_2$, and the blue spectrum denotes $^{18}O_2$. Note: $^{18}O_2$ spectra contain a small amount of isotopic $^{16}O_2$. Inset: $^{16}O_2$ and $^{18}O_2$ isotope comparison for R = Me_2N at 77 K in THF-d_8. Excitation at 380 nm.

ν_{Cu-Cu} = 275 cm^{-1} ($^{16,18}\Delta = 0$ cm^{-1}; Figure 3), while, for the bis-μ-oxo-dicopper(III) isomer, the ν_{Cu-O} peak is split into a doublet of peaks at ν = 579 and 590 cm^{-1} (ν_{avg} = 585 cm^{-1}). Upon $^{18}O_2$ substitution, this doublet collapses to a single peak at ν = 559 cm^{-1}, allowing assignment of the peaks in the $^{16}O_2$ spectrum as a Fermi doublet and determination of $^{16,18}\Delta = -26$ cm^{-1}. Also for the $[\{(MeO\text{-}MePY2)Cu\}_2(O_2)]^{2+}$ bis-μ-oxo-dicopper(III) complex, ν_{Cu-NPY} = 493 cm^{-1} ($^{16,18}\Delta = 0$ cm^{-1}) and ν_{Cu-N} = 530 cm^{-1} ($^{16,18}\Delta = 0$ cm^{-1})

The rRaman spectrum for R = Me_2N contains the side-on peroxo-dicopper(II) bands ν_{O-O} = 729 cm^{-1} ($^{16,18}\Delta = -40$ cm^{-1}) and ν_{Cu-Cu} = 275 cm^{-1} ($^{16,18}\Delta = 0$ cm^{-1}; Figure 4). The bis-μ-oxo-dicopper(III) isomer for this ligand is highly unstable toward decomposition (and oxidative attachment of solvent as a substrate)[31] to a product with a broad band in the 500−600 cm^{-1} region, making observation of ν_{Cu-O} stretch for this species difficult. However, comparison of the $^{16}O_2$ and $^{18}O_2$ spectra indicates the presence of an oxygen isotope sensitive band shifting in this region (Figure 4, inset). Further, the absorption spectrum for R = Me_2N, which was collected at much lower concentrations (at which the complex is more stable)

Table 3. Resonance Raman Stretching Frequencies for the R−MePY2 Ligand Series

	side-on peroxo					bis-μ-oxo				
	ν_{O-O}					ν_{Cu-O}				
	$^{16}O_2$	$^{18}O_2$	$\Delta\nu$	ν_{Cu-PY}	ν_{Cu-Cu}	$^{16}O_2$	$^{18}O_2$	$\Delta\nu$	ν_{Cu-N}	ν_{Cu-PY}
R = H	729	689	40	~275	265, 289 av = 277	587	561	26	538	491
R = MeO	728	689	39	295	275	590, 579 av = 585	559	26	530	493
R = NMe_2	729	689	40	305	275	~548	~523	25		

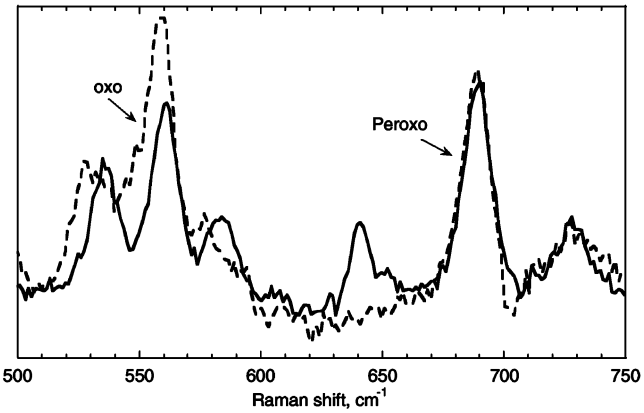

Figure 5. Solvent subtracted $^{18}O_2$ resonance Raman comparison of the side-on peroxo-dicopper(II) and bis-μ-oxo-dicopper(III) complex intensities for the $[\{(R-MePY2)Cu\}_2(O_2)]^{2+}$ series in THF-d_8 at 77 K. Intensity comparison for R = H (——) and R = MeO (- - - - -). Excitation at 407 nm.

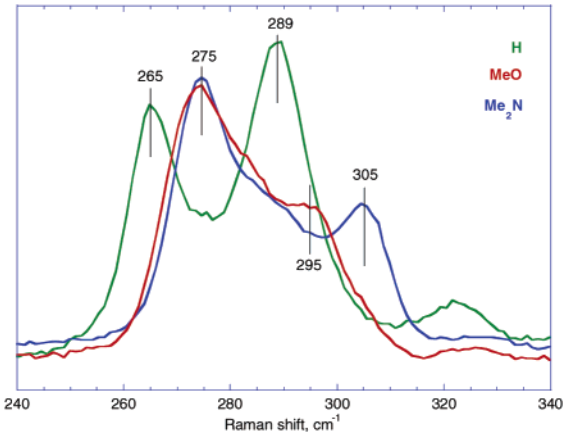

Figure 6. Resonance Raman spectra (77 K) of the $[\{(R-MePY2)Cu\}_2(O_2)]^{2+}$ series in THF-d_8 at 380 nm excitation. For the R−MePY2 series, the green spectrum denotes R = H, the red spectrum denotes R = MeO, and the blue spectrum denotes R = Me_2N.

relative to the rRaman samples, confirms the formation of both isomers with this ligand (see Supporting Information Figures S3 and S6−S8).

An overlay plot of the $^{18}O_2$ spectra of $[\{(R-MePY2)Cu\}_2(O_2)]^{2+}$ for R = H and MeO is shown in Figure 5.[43] The relative amount of bis-μ-oxo-dicopper(III) complex in the equilibrium mixtures was determined by integrating the Raman peak intensities of the $^{18}O_2$ ν_{O-O} and ν_{Cu-O} bands at ~690 cm^{-1} and ~560 cm^{-1}, respectively, and scaling the Raman peroxo peaks as in Figure 5. Changing the R−MePY2 substituent from R = H to MeO shifts the equilibrium such that the relative amount of bis-μ-oxo-dicopper(III) complex formed increases ~37%.[44] Me_2N−MePY2 appears to form more bis-μ-oxo-dicopper(III) complex than R = MeO. The rRaman data for R = Me_2N (Figure 4) show that the bis-μ-oxo-dicopper(III) isomer does exist, and fitting the absorption spectra for side-on peroxo-dicopper(II) and bis-μ-oxo-dicopper(III) complex peaks shows a decreasing ratio of side-on peroxo/bis-μ-oxo peak areas on going from R = H to MeO and MeO to Me_2N (see Supporting Information Figures S6−S8).[45]

(43) Directly comparing the $^{16}O_2$ intensities is difficult due to Fermi resonance in the R = MeO spectrum.

(44) The 37% increase of bis-μ-oxo-dicopper(III) complex on going from R = H to MeO should be considered a minimum value. The absorption data in Table 1 indicate that the UV−vis peaks of the side-on peroxo-dicopper(II) complex increase more in intensity than those of the bis-μ-oxo-dicopper-(III) complex. The resonance Raman intensity scales to ϵ^2, and this estimate involves scaling the entire spectrum to the O−O stretch of the side-on peroxo-dicopper(II) complex. In addition, the peak at 640 cm^{-1} is present in the $^{18}O_2$ spectrum of $[\{(H-MePY2)Cu\}_2(O_2)]^{2+}$, but is not present in the corresponding $^{16}O_2$ spectrum (Figure 2). It likely acquires intensity by mixing with the ~690 cm^{-1} side-on peroxo-dicopper(II) complex peak. Including this in the normalization would involve an area summation of the 640 and 690 cm^{-1} peaks, decreasing the relative intensity of the side-on peroxo-dicopper(II) peak in this figure.

(45) This trend is also observed in CO binding studies and electrochemical data (see refs 16 and 17) and Cu−N_{PY} satellite peaks (vide infra).

An interesting trend is also observed over the R−MePY2 series for the side-on peroxo-dicopper(II) component features in the 260−300 cm^{-1} region (Figure 6). The spectra for both R = MeO and Me_2N are characterized by a single intense ν_{Cu-Cu} peak at 275 cm^{-1}, with a weaker satellite peak at a higher stretching frequency which may be assigned as a Cu−N_{PY} stretch of the side-on peroxo species.[46] The ν_{Cu-NPY} band is highest in frequency (305 cm^{-1}) for R = Me_2N. This band shifts down in frequency for R = MeO (ν = 295 cm^{-1}), becoming a shoulder on the more intense ν_{Cu-Cu} peak. The spectrum for R = H shows two intense, oxygen isotope independent peaks at 265 and 289 cm^{-1} (av = 277 cm^{-1}). These peaks are assigned as a Fermi doublet arising from resonant overlap between the ν_{Cu-Cu} band and a ν_{Cu-NPY} peak further downshifted relative to the R = Me_2N and MeO complexes.

Discussion

Substituents are observed to affect the frequencies of the O−O and Cu−O stretches in $[\{(R-TMPA)Cu^{II}\}_2(O_2)]^{2+}$ (Figure 1), in a manner that directly reflects the donor strength of the substituent. As the R− substituent on the pyridine ring is varied from H to MeO to Me_2N, the ability of the R−TMPA ligand to donate electron (e^-) density to Cu(II) is increased. The increased ligand donation decreases the amount of σ e^- donation to Cu(II) from the π^*_σ orbital of the peroxide bridge (Scheme 1, top). Thus, the Cu−O bond strength decreases, and because decreased σ donation from peroxide results in more e^- density in the peroxide π^* orbitals (which are antibonding with respect to the O−O bond), the O−O bond strength and ν_{O-O} decrease as well.

(46) Henson, M. J.; Mahadevan, V.; Stack, T. D. P.; Solomon, E. I. *Inorg. Chem.* **2001**, *40*, 5068.

In support of this being an electronic effect, the ν_{Cu-Nax} peak positions measurably decrease as R is varied from H to MeO to Me_2N (Table 2). A mass effect would not be expected here as varying R only adds mass to the pyridine rings, which are in the equatorial plane of the trigonal bipyramid. However, increasing the N-donor strength of the pyridines would add electron density to Cu(II) atoms, which in turn would limit electron density donation from the axial nitrogen and weaken the $Cu-N_{ax}$ bond.

Electronic substituent effects are also observed to affect the side-on peroxo-dicopper(II) and bis-μ-oxo-dicopper(III) complex peak frequencies as well as the bis-μ-oxo-dicopper(III)/side-on peroxo-dicopper(II) equilibrium in the MePY2 ligand system. As the pyridine substituent is varied from H to MeO to Me_2N (increasing the strength of the N-donor), ν_{Cu-O} for the bis-μ-oxo-dicopper(III) complexes decreases from 587 cm^{-1} for R = H to ~548 cm^{-1} for R = Me_2N.[47] That the substituent effects are electronic in nature and not simply mass effects, as suggested by Holland, et al.,[21] can be seen from the Cu−N shifts in the side-on peroxo-dicopper(II) and bis-μ-oxo-dicopper(III) complexes. Figure 6 for the side-on peroxo-dicopper(II) complex shows the $Cu-N_{PY}$ stretch *increasing* as the strength of the N-donor (and relative mass) is increased. This is opposite of the expected trend if a mass effect was dominant. For the bis-μ-oxo-dicopper(III) complex, an upward shift in the $Cu-N_{PY}$ stretching frequencies and a downward shift in the Cu−N stretches are observed (Table 3) as R is varied from H to MeO. This is to be expected for an electronic effect. As the strength of the N-donor is increased, the $Cu-N_{PY}$ bond would strengthen, shifting to a higher frequency. However, as the pyridine donates added electron density to the Cu atom, less electron density will be donated by the tertiary nitrogen ligand, which will weaken the Cu−N bond and lower ν_{Cu-N}.

However, ν_{Cu-O} does shift downward slightly as R is varied from H to MeO, which has been ascribed to a mass effect in similar systems.[21] A normal coordinate analysis (NCA) was performed to address the direct effect of the Cu−N and $Cu-N_{PY}$ bonds on Cu−O bonding. The lack of mixing between the Cu−O and Cu−N modes is evident by (1) the $^{18}O_2$ insensitivity of ν_{Cu-N} and ν_{Cu-NPY} for R = H and MeO (see Figures 2 and 3, respectively), indicating little to no mixing with oxygen containing modes (When R = H, $^{16,18}\Delta = 2.5$ and 1.0 cm^{-1} for ν_{Cu-N} and ν_{Cu-NPY}, respectively, in the NCA fit. When R = MeO, $^{16,18}\Delta = 1.4$ and 1.8 cm^{-1} for ν_{Cu-N} and ν_{Cu-NPY}, respectively.); (2) the normal coordinate fit shows negligible mixing between the ν_{Cu-N} and ν_{Cu-NPY} modes; (3) NCA shows that the mass effect on the $Cu-N_{PY}$ bond on changing from R = H to MeO would be on the order of 60−70 cm^{-1} rather than the observed shift of $\Delta = +2$ cm^{-1} opposite the mass effect. By fitting the observed frequency shifts for R = H and MeO, the NCA shows that strengthening the N-donor to R = MeO weakens the Cu−O and Cu−N bonds and greatly strengthens the $Cu-N_{PY}$ bond (Table 4). Thus, as the N-donor strength of the pyridine is increased, the tertiary nitrogen and oxygen ligands become poorer donors to the copper.

(47) Crystal structures of the bis-μ-hydroxo-dicopper(II) complexes, $[\{(R-MePY2)Cu\}_2(OH)_2]^{2+}$ (Karlin, et al. unpublished results), show that, for R = H and MeO, there is one equatorial and one axial pyridine ligand. However, for R = Me_2N, both pyridine ligands are equatorial and the tertiary nitrogen is axial. This may account for the large difference in ν_{Cu-O} for R = Me_2N versus R = H and MeO.

Table 4. Force Constant Fits (mdyn/Å) for R = H, MeO in the MePY2 Ligand System

	force constants	
mode	R = H	R = MeO
Cu−O stretch	3.62	3.58
Cu−PY stretch	2.63	3.60
Cu−N stretch	2.27	2.19
O−Cu−N bend	0.35	0.35

Table 5. Atomic Contributions to Selected Molecular Orbitals[a]

	side-on peroxo (HOMO = σ_u^*; LUMO = π_σ^*)			end-on peroxo (LUMO = π_σ^*)			bis-μ-oxo (LUMO = σ_u^*; LUMO + 1 = π_σ^*)		
	Cu	O	N	Cu	O	N	Cu	O	N
LUMO + 1							58	22	9
LUMO	35	12	4	35	10	9	56	31	6
HOMO	38	4	5						

[a] Values are scaled to reflect the number and type of equatorial N-donors.

Electronic substituent effects also affect the amount of bis-μ-oxo-dicopper(III) isomer present, increasing it along the series R = H, MeO, Me_2N (Figure 5), which reflects relative thermodynamic stabilities. Although the R = H ligand dominantly forms the side-on peroxo-dicopper(II) isomer, increasing the N-donor ability and thereby increasing e^- density donation to the copper preferentially stabilizes the Cu(III) centers of the bis-μ-oxo-dicopper(III) isomer for R = MeO and Me_2N. Thus, the equilibrium shifts toward the bis-μ-oxo-dicopper(III) isomer due to *electronic rather than steric effects*.

The effect of additional electron density donation to the Cu(II) centers can be extrapolated from examining atomic contributions to the relevant antibonding π and σ molecular orbitals. These contributions have been previously calculated for similar systems and are summarized in Table 5.[26,27,29] These results reveal that the end-on peroxo-dicopper(II) and bis-μ-oxo-dicopper(III) isomers have higher contributions from the nitrogens to the antibonding LUMO molecular orbitals. Thus, increased N-donor strength would be expected to have a greater effect on the core Cu_2O_2 vibrational frequencies of the end-on peroxo-dicopper(II) and bis-μ-oxo-dicopper(III) complexes than on those of the side-on peroxo-dicopper(II) complex. In particular, this correlates with the greater sensitivity of the bis-μ-oxo-dicopper(III) complex than the side-on peroxo-dicopper(II) complex to N-donor strength and stabilization.

While the amount of bis-μ-oxo-dicopper(III) isomer formed is observed to increase with the donor strength of the endogenous ligand system, the lack of a substituent-dependent shift in the O−O stretching frequency for R = H (ν_{O-O} = 729 cm^{-1}), MeO (ν_{O-O} = 728 cm^{-1}), or Me_2N (ν_{O-O} = 729 cm^{-1}) in the side-on peroxo-dicopper(II) complex (Table 3) indicates little change in the extent of Cu_2/O_2 back-bonding in the three complexes studied.

To explore the insensitivity of the side-on peroxo ν_{O-O} to N-donor strength, DFT calculations were performed on a side-on peroxo $[\{(NH_3)_3Cu^{II}\}_2(O_2)]^{2+}$ core molecule (as both a delocalized and localized singlet, the latter to better clarify the effect of σ^*_u mixing) with varied equatorial ligation. The effect of increasing N-donor strength was modeled by shortening the $Cu-N_{eq}$ bond of a geometry optimized structure by 0.05 Å and performing a single-point calculation. The localized singlet HOMO (σ^*_u) shows an increase in N contribution, a decrease

Table 6. Percent Change in Atomic Contributions of the Localized Singlet State of $[\{(NH_3)_3Cu^{II}\}_2(O_2)]^{2+}$ when Shortening the Equatorial Cu−N Bonds (Δ = (Short CuN) − (Long CuN))

	atomic contribution	
atoms	HOMO	LUMO
O	0.29%	−7.04%
Cu	−3.90%	3.13%
N_{eq}	3.59%	3.88%

in Cu contribution, and a negligible effect of the O contribution on going from the long to the short Cu−N_{eq} bond (Table 6). This indicates that σ^*_u back-bonding from the Cu to the peroxo is not significantly affected by the strength of the N-donor. In contrast, in the LUMO (π^*_σ antibonding), the O contribution decreases while the N and Cu contributions increase, indicating less Cu−O interaction and an expected decrease in ν_{Cu-O}.[48]

Revisiting the peroxide π^* donation and σ^* back-bonding model,[25,30] we observed that the amount of back-bonding into the peroxide is dependent upon the strong σ donation from the π^*_σ to the Cu(II) atoms (facilitated by four Cu−O bonds; see Scheme 1, bottom left). As the strength of the N-donor increases, more electron density is donated to the Cu(II) atoms. This decreases the positive charge on the Cu(II) atoms. As a result, less charge is donated from the peroxide π^*_σ orbitals (Scheme 1, bottom left). More electron density on the Cu(II) decreases the effective charge of the Cu(II) atoms, thereby increasing the d-orbital energies, which should increase the back-bonding from the copper to the peroxide σ^*_u orbitals (Scheme 1, bottom right). However, the increased negative charge on the peroxide adversely affects the back-bonding due to the energetically disfavored process of donating additional electron density to an already more negative peroxide. Any net effect would be further mitigated by the presence of only one equatorial N-donor substituent per Cu for the MePY2 ligand.

(48) A decrease in the Cu−O stretching frequency of the side-on peroxo-dicopper(II) complex would not be observed in the rRaman spectrum. The rRaman observable "Cu−Cu" stretch at ~280 cm^{-1} would not be expected to change even with a dramatic change in the Cu−O force constant. (See: Baldwin, M.; et al. *J. Am. Chem. Soc.*, **1992**, *114*, 10421.)

In summary, substituted end-on and side-on bridged peroxo-dicopper(II) and bis-μ-oxo-dicopper(III) complexes were studied to gain a better understanding of electronic effects on Cu_2O_2 bonding and on the side-on peroxo-dicopper(II)/bis-μ-oxo-dicopper(III) equilibrium. Increasing the endogenous N-donor strength in the $[\{(R-TMPA)Cu^{II}\}_2(O_2)]^{2+}$ ligand series was observed to affect σ donation to copper, weakening the Cu−O and O−O bonds. Increasing the N-donor strength also weakens the Cu−O bond in the bis-μ-oxo-dicopper(III) complex in the $[\{(R-MePY2)Cu\}_2(O_2)]^{2+}$ ligand series. For the side-on peroxo-dicopper(II) model, N-donor interactions were determined to have little direct effect on the bonding associated with its unique electronic structure. Rather, the equilibrium is shifted due to the thermodynamic effect of increased N-donor strength better stabilizing the high-valent bis-μ-oxo-dicopper(III) species. Thus, the side-on peroxo-dicopper(II)/bis-μ-oxo-dicopper(III) equilibrium is shifted due to electronic rather than steric effects.

Acknowledgment. This work was supported by grants from the N.I.H.: DK31450 (E.I.S.) and GM28962 (K.D.K.). M.A.V. has a predoctoral research fellowship from the NSF. Special thanks to Peng Chen and Andrew Skulan for their help with the normal coordinate analysis.

Supporting Information Available: $^{16}O_2$ and $^{18}O_2$ isotope comparison of resonance Raman spectra of $[\{(R-TMPA)Cu^{II}\}_2(O_2)]^{2+}$ in Et_2O at 77 K (R = MeO, Me_2N), UV−vis spectra of $[\{(R-TMPA)Cu^{II}\}_2(O_2)]^{2+}$, $^{16}O_2$ and $^{18}O_2$ isotope comparison of resonance Raman spectra of $[\{(MeO-TMPA)Cu^{II}\}_2(O_2)]^{2+}$, solvent subtracted comparison plot of $^{16}O_2$ resonance Raman spectra of $[\{(R-MePY2)Cu\}_2(O_2)]^{2+}$, UV−vis peak fits for $[\{(R-MePY2)Cu\}_2(O_2)]^{2+}$ complexes (R = H, MeO, Me_2N), Cartesian input coordinates for Gaussian calculations, normal coordinate analysis input files and procedures, and brief TMPA and MePY2 ligand syntheses. This material is available free of charge via the Internet at http://pubs.acs.org.

JA0276366